

A sample of X-ray emitting normal galaxies from the BMW – HRI Catalogue

Marzia Tajar^{1,2}, Ginevra Trinchieri¹, Anna Wolter¹, Sergio Campana¹, Alberto Moretti¹, Gianpiero Tagliaferri¹

¹ INAF-Osservatorio Astronomico di Brera, via Brera 28, 20121 Milano Italy

² Università di Milano - Bicocca, Dipartimento di Fisica, P.zza della Scienza 3, 20126 Milano Italy

Draft: November 29, 2018

Abstract. We have obtained a sample of 143 normal galaxies with X-ray luminosity in the range $10^{38} - 10^{43}$ erg s⁻¹ from the cross-correlation of the ROSAT HRI Brera Multi-scale Wavelet (BMW – HRI) Catalogue with the Lyon-Meudon Extragalactic Database (LEDA). We find that the average X-ray properties of this sample are in good agreement with those of other samples of galaxies in the literature. We have selected a complete flux limited serendipitous sample of 32 galaxies from which we have derived the logN-logS distribution of normal galaxies in the flux range $1.1 - 110 \times 10^{-14}$ erg cm⁻² s⁻¹. The resulting distribution is consistent with the euclidean –1.5 slope. Comparisons with other samples, such as the Extended Medium Sensitivity Survey, the ROSAT All Sky Survey, the XMM - Newton/2dF survey and the *Chandra* Deep Field Survey indicate that the logN-logS distribution of normal galaxies is consistent with an euclidean slope over a flux range of about 6 decades.

Key words. X-ray – galaxies: general – X-ray surveys

1. Introduction

Detailed X-ray studies of normal galaxies have been possible only with the advent of imaging instruments aboard the *Einstein* observatory. The *Einstein* results were summarized in the catalogue and atlas published by Fabbiano et al. (1992), who constructed a large homogeneous sample of 493 galaxies, included in either A Revised Shapley-Ames Catalog of Bright Galaxies (Sandage & Tammann, 1981), or in the Second Revised Catalog of Bright Galaxies (de Vaucouleurs et al., 1976), both targets and serendipitously detected in *Einstein* fields. While representative of the galaxy population (see e.g. Shapley et al., 2001; Eskridge et al., 1995), it was not constructed to be a complete, unbiased sample, and it is likely to contain unknown selection biases.

Elliptical galaxies were found to retain large amounts ($10^8 - 10^{11}$ M_⊙) of hot gas (T $\sim 10^7$ K) whose thermal emission dominates their X-ray luminosities, while in normal spirals the integrated contribution of the evolved stellar sources, such as supernova remnants and X-ray binaries, is generally the dominant component (see Fabbiano, 1989; Fabbiano et al., 1992; Kim et al., 1992). Extended emission from a hot, gaseous component in spiral galaxies was detected only in some cases (Fabbiano & Trinchieri,

1987; Vogler & Pietsch, 1996; Trinchieri et al., 1988), or associated with starburst activity.

Subsequent observations of individual sources made by *ROSAT* and *ASCA* confirmed most of the *Einstein* results and added interesting information on the X-ray properties of normal galaxies (see among others Roberts & Warwick, 2000; Read et al., 1997; Brown & Bregman, 1998; Beuing et al., 1999) in the local universe.

With the launch of *XMM - Newton* and *Chandra*, the study of the X-ray properties of “normal” galaxies at intermediate ($z \sim 0.1$) or cosmological distances (Brandt et al., 2001; Hornschemeier et al., 2002, 2003; Georgakakis et al., 2003, 2004a,b; Norman et al., 2004) was made possible, thanks to significantly improved sensitivity, spatial and spectral resolution of the instruments. In spite of the large number of papers, however, a truly complete sample of X-ray emitting normal galaxies in the local universe with a significant number of objects has not been properly discussed in the literature so far. Georgakakis et al. (2003) give galaxy number density at $F_{0.5-2} \sim 7 \times 10^{-16}$ erg cm⁻² s⁻¹ from stacking analysis, while Georgakakis et al. (2004a) present a sample of 26 X-ray sources detected in an area of ~ 2.5 deg⁻², of which only 2 are however classified as normal galaxies. Only recently Georgakakis et al. (2004b) have presented a larger

sample of 11 normal galaxies detected in an area of ~ 4.5 deg $^{-2}$.

Two other samples of “normal” galaxies are available in the literature, selected in the *Chandra* Deep Fields (Hornschemeier et al., 2003; Norman et al., 2004). However their median redshifts ($z = 0.297$, Hornschemeier et al. (2003) and $z = 0$ to $z = 1.3$, Norman et al. (2004)) indicates that they should not be considered as “local”.

The large database provided by ROSAT has been exploited only marginally to derive unbiased and complete sample of galaxies. Zimmermann et al. (2001) have selected a sample of *candidate normal galaxies* from the *ROSAT* All Sky Survey (RASS) Bright Source Catalogue (Voges et al., 1999) above a flux limit of about 10^{-12} erg cm $^{-2}$ s $^{-1}$ (0.1 – 2.4 keV band). A few samples have been derived from the *ROSAT* Position Sensitive Proportional Counter (PSPC) pointed observations such as the WGA (White, Giommi, & Angelini, 1994) and the ROSPSPC (*ROSAT* team 2001), and a new catalogue of galaxies is in progress (G. Peres, private communication). Here we exploit the potential provided by the Brera Multi-scale Wavelet (BMW – HRI) catalogue (Panzera et al., 2003) to extract a sample of normal galaxies, as we discuss in the next sections. While the PSPC is probably more efficient at detecting faint and extended sources such as galaxies, the sharp core of the HRI point spread function allows the detection of sources in more crowded fields and to establish the extension for bright small-size sources, providing a good complement to the PSPC data.

2. The sample

In order to create a complete, serendipitous sample of galaxies with X-ray emission, we made use of X-ray data from the BMW *ROSAT* HRI catalogue and optical data from LEDA (Lyon-Meudon Extragalactic Database). The BMW – HRI catalogue consists of 29089 X-ray sources detected in 4303 *ROSAT* HRI pointed fields with exposure times longer than 100 s using a multiscale wavelet algorithm (Lazzati et al., 1999; Campana et al., 1999; Panzera et al., 2003). Sources detected with a significance $\geq 4.2\sigma$ are contained in the catalogue, that provides name, position, count rate, flux and extension along with the relative errors. In our study we used the full catalogue, but we excluded X-ray sources in the Trapezium field, which is a rich stellar cluster in the Milky Way, where the high density of the X-ray sources would prevent proper optical identifications. The BMW – HRI catalogue can be searched via the HEASARC Browse¹ or via the Brera Observatory web site.²

¹ <http://heasarc.gsfc.nasa.gov/cgi-bin/W3Browse/w3browse.pl>

² <http://www.merate.mi.astro.it:8081/interroga/dbServer?cmd=bmw2>

Created in 1983 at Lyon Observatory, LEDA³ has been the first database of extragalactic objects and it is continuously updated. It gives a free access to the main astrophysical parameters (coordinates, morphological type, diameter and axis ratio, apparent magnitudes and colors, radial velocity, surface brightness, etc) for about 10^6 galaxies over the whole sky. The completeness in apparent B – magnitude is satisfied up to $m_B = 15.5$ (see Paturel et al., 1997).

To obtain a representative sample of galaxies we started from the BMW – HRI catalogue and included only serendipitous detections, avoiding the targets. We chose a 3' radius to define the typical region of the target, and selected only sources at off-axis angles $\theta > 3'$. In spite of their off-axis location, we had to exclude 12 additional sources that were targets of the observations. We then cross - correlated the positions of the X-ray sources in the BMW – HRI catalogue with those of galaxies present in the LEDA database version of 1999, with a tolerance of 20'', which should be a reasonable guess to detect extended objects like galaxies and to avoid most of chance coincidences. This criterium is not appropriate for very extended galaxies (like e.g. M 31 or M 33), where a large number of sources is detected at distances significantly larger than our tolerance radius. Therefore we could be selecting against large size galaxies, if there is no source within a distance of $\sim 20''$ from the nucleus. However, this should not be a concern in this study, since the surface density of large galaxies is small: in particular, in the LEDA catalog, the density of galaxies with $D_{25} > 3'$ is $< 3 \times 10^{-2}$ deg $^{-2}$, which implies about < 10 in the area we surveyed.

To check the goodness of our choice, we plot in Fig. 1 the relative shifts between optical and X-ray positions. We use only point-like X-ray sources because in extended sources the association with a single optical object could be misleading (e.g. in groups and pairs). About 90% of identifications are within 13'' (represented by the dashed circle in Fig. 1).

This is in good agreement with the HRI positional uncertainty, since the best attitude solution guarantees that on average known objects are detected within 10'' of their catalog position, although with possible additional discrepancy mainly in declination (see the *ROSAT* Handbook e.g. at <http://heasarc.gsfc.nasa.gov/docs/rosat/ruh/handbook/handbook.html>). We verified that all X-ray sources with X-ray/optical off-set $> 10''$ are still within the galaxy (i.e. D_{25}). We conclude that the association of the X-ray sources with galaxies found by the cross-correlation is sound on positional grounds.

The cross-correlation yields 399 X-ray sources associated with 281 galaxies. Being constructed field-by-field, the BMW – HRI catalogue contains multiple detections of the same source. Therefore we only have 283 distinct X-

³ There exist several mirrors to access LEDA; we used the OAB one, <http://www.brera.mi.astro.it/hypercat/>

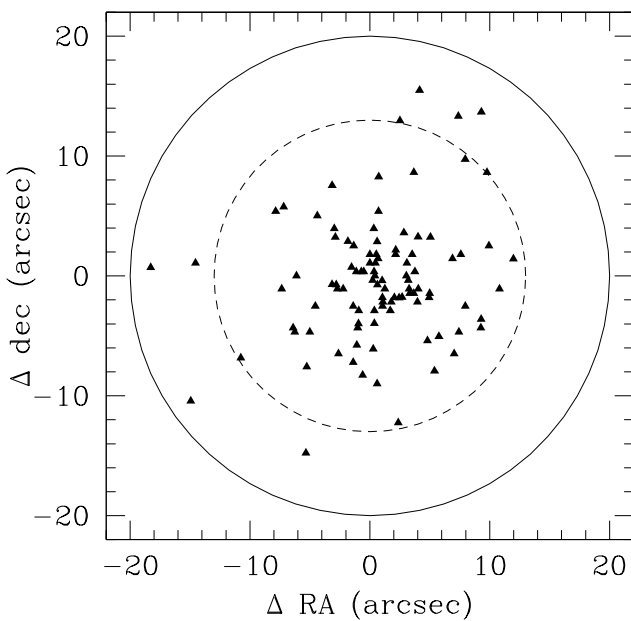


Fig. 1. Displacement between optical and X-ray positions for point-like sources in the total sample. The solid circle refers to the cross - correlation radius of 20"; the dashed one, with 13" radius, contains about 90% of the identifications.

ray sources associated with galaxies (two distinct sources but of different extent are associated with both NGC 1399 and M 86; we list them in Table 1, but we consider only the largest one for computing fluxes and luminosities).

To check the results of the cross-correlation, we inspected HRI images for each source and obtained information from the NASA/IPAC Extragalactic Database (NED) to a) eliminate spurious coincidences [15 sources], b) eliminate AGNs [47 objects] and c) select clusters [57 objects].

a . We eliminated a source when the obvious optical counterpart was not a LEDA galaxy, but a background or foreground object. This was checked both using NED and the X-ray/optical contour maps.

b . We excluded objects classified in Véron-Cetty & Véron Catalogue (2001) as Seyfert 1 galaxies, QSOs, BL Lacs or AGNs. For Seyfert 2 galaxies, the X-ray emission could have a non nuclear origin, so we eliminated them when we saw from images that the X-ray emission was point-like and well centered on the nucleus, while we retained those for which we found an extended emission.

We also retained starburst galaxies, LINERs and objects that we know from the literature could have a nuclear source but also non - nuclear X-ray emission (e.g. NGC 3079).

c . Several galaxies lie inside a cluster: we inspected X-ray images and we eliminated those objects whose X-ray emission was indistinguishable from the cluster's, but we retained galaxies for which emission

clearly associated with the galaxy is detected above the cluster background (see e.g. PGC 12350 in Fig. 2). We retained galaxies in poor groups even when they are the brightest member since there is still ambiguity in the literature between emission from bright early-type galaxies and groups, which are often analyzed in the same context (see e.g. Mamon, 1992; Dell'Antonio et al., 1994; Pildis et al., 1995; Ponman et al., 1996; Mahdavi et al., 1997; Mulchaey & Zabludoff, 1998; Helsdon & Ponman, 2000; Mulchaey et al., 2003; Osmond & Ponman, 2004; Helsdon & Ponman, 2003; Jones et al., 2003).

Moreover, in 5 cases the same X-ray source was associated with two or more galaxies in a pair or in a group: since we could not discriminate on a positional basis, we chose the brightest galaxy in the pair or in the group.

These selection criteria yielded a total of 195 X-ray sources (including multiple detections) associated with 143 galaxies whose properties are listed in Table 1, available in electronic form. We report here the first page as an example. Column (1) gives the BMW – HRI name of the source, columns (2) and (3) the position of the X-ray peak, column (4) labels the source as point-like (p) or extended (e), column (5) gives the radius in which we computed count rates for extended sources (see section 3), column (6) the major semiaxis of the ellipse, for extended X-ray sources for which count rates have been computed in elliptical regions (see section 3), column (7) the minor semiaxis of the ellipse, column (8) the LEDA galaxy associated to the X-ray source, column (9) the name of the galaxy in other common catalogues (e.g. NGC), column (10) the morphological type, column (11) the distance of galaxy, column (12) the apparent B - magnitude corrected for galactic extinction, inclination and redshift effects (see Paturel et al., 1997), columns (13) and (14) the HRI count rate and error, columns (15) and (16) the X-ray flux and error (0.1 – 2 keV; count rates and fluxes have been recomputed with respect to values reported in the BMW – HRI catalogue; see section 3 for details), column (17) the logarithm of X-ray luminosity and column (18) specifies whether the galaxy is in the complete subsample (c), in cluster (Cl) or in group (Gr).

Information about magnitudes and redshifts are from LEDA and NED except for 3 objects that we observed ourselves (see section 5). We calculated distances from redshifts, assuming $H_0 = 50 \text{ km s}^{-1} \text{ Mpc}^{-1}$; when the heliocentric radial velocity of galaxy was less than 3000 km s^{-1} , however, we used distances from Nearby Galaxy Catalogue (Tully, 1988) corrected for $H_0 = 50 \text{ km s}^{-1} \text{ Mpc}^{-1}$.

One hundred and sixteen of the 143 galaxies have redshift and magnitude (including our observations). Nineteen galaxies have m_B and no z , 3 have z and no m_B and 5 have neither z nor m_B . The redshift distribution ranges from $z = 0$ from $z \sim 0.15$, but $\sim 90\%$ of galaxies have $z < 0.07$.

(1)	(2)	(3)	(4)	(5)	(6)	(7)	(8)	(9)	(10)	(11)	(12)	(13)	(14)	(15)	(16)	(17)	(18)
BMW000523.9+161307	00 05 23.83	+16 13 11.3	e	52			PGC 0000372		698			15.74	2.49	7.40	1.17	43.59	Cl
BMW002055.1+215208	00 20 55.43	+21 51 52.2	p				PGC 0001333 IC 1543		Sbc	112	14.54	7.63	1.11	3.58	0.52	41.71	c
BMW002055.2+215208																	
BMW002549.3-453227	00 25 49.26	-45 32 26.5	p				PGC 0143535		Sab		16.57	18.64	3.16	7.64	1.30		
BMW002950.2-405630	00 29 50.99	-40 56 37.9	p				PGC 0130966 DUKST 294-9		Sc	241	15.35	19.06	2.31	7.81	0.95	42.72	c
BMW003652.3-333310	00 36 52.82	-33 33 14.7	p				PGC 0002204 ESO 350-IG38		S?	123	14.96	2.74	0.43	1.12	0.14	41.27	c
BMW003918.5+030220	00 39 18.47	+03 02 14.8	p				PGC 0002362 NGC 194		E	103	13.09	14.75	1.94	6.49	0.85	41.89	c; Gr
BMW003948.3+032219	00 39 48.77	+03 22 21.0	p				PGC 0002401 UM 57				6.15	0.49	2.70	0.22			
BMW004242.0+405154	00 42 42.48	+40 51 52.6	e	60			PGC 0002555 NGC 221		E	1	8.18	52.44	1.06	26.75	0.54	38.52	Gr
BMW010716.2+323117	01 07 16.20	+32 31 16.6	p				PGC 0003966 NGC 379		SO	110	13.48	1.37	0.35	0.67	0.17	40.98	Gr
BMW010717.4+322857	01 07 17.76	+32 28 57.0	p				PGC 0003969 NGC 380		E	88	13.24	4.19	0.50	2.06	0.24	41.26	Gr
BMW010717.8+322857																	

- (1) BMW – HRI source name
- (2) X-ray coordinates: RA (J2000)
- (3) X-ray coordinates: Dec (J2000)
- (4) X-ray source point-like (p) or extended (e)
- (5) Radius of circle in which count rates were computed, for extended X-ray sources
- (6) Major semiaxis of ellipse in which count rates were computed, for some peculiar extended X-ray sources
- (7) Minor semiaxis of ellipse in which count rates were computed, for some peculiar extended X-ray sources
- (8) LEDA galaxy associated
- (9) Other galaxy name
- (10) Morphological galaxy type
- (11) Galaxy distance (Mpc)
- (12) Apparent B - magnitude
- (13) X-ray count rate (10^{-3} count s $^{-1}$)
- (14) X-ray count rate error (10^{-3} count s $^{-1}$)
- (15) X-ray flux (0.1 – 2 keV band; 10^{-13} erg cm $^{-2}$ s $^{-1}$)
- (16) X-ray flux error (0.1 – 2 keV band; 10^{-13} erg cm $^{-2}$ s $^{-1}$)
- (17) Logarithm of X-ray luminosity (0.1 – 2 keV band; erg s $^{-1}$)
- (18) Notes: c if the galaxy is in the complete subsample, Cl if in cluster, Gr if in group

Table 1. First page of Table of the total sample, available in electronic form.

2.1. The complete serendipitous subsample

To study the general properties of the sample we need to derive a subsample with well known completeness criteria and limits. To this end we constructed a complete sample with both X-ray and optical flux limits. We must consider both the X-ray and the optical completeness criteria. The X-ray completeness is related to the BMW – HRI catalogue, that includes all sources with a significance $\geq 4.2\sigma$. To take into account the optical limits, we excluded galaxies fainter than $m_B = 15.5$ (the completeness limit assumed for the LEDA Catalogue, see Paturel et al., 1997).

We have also excluded objects at low galactic latitude ($|b| \leq 10^\circ$) to avoid source confusion in the galactic plane and X-ray sources with off-axis angle $\theta \geq 18'$ to match the circular HRI field of view used in the sky coverage computation (see section 7).

The resulting sample of 96 objects is complete both in X-ray and optical, at the given limits. However, since galaxies are often in agglomerates, some of them are expected to be related to the targets and therefore not truly serendipitous. We therefore excluded all sources known to be associated with the target (e.g. galaxies in pairs, groups or clusters; 52 objects). When an association was not documented (e.g. from NED, LEDA) we conservatively excluded galaxies at the same redshift of the target (12 objects).

The complete, serendipitous sample of 32 galaxies thus obtained is given in Table 3 and will be used to calculate the logN-logS distribution in the local universe ($z < 0.07$), as will be described in detail in section 7.

3. X-ray characterization

The BMW – HRI catalogue provides count rates derived using the wavelet algorithm, in an automated way and under particular assumptions (for details, see Lazzati et al., 1999; Campana et al., 1999). We verified that, while count rates are correctly computed for point-like sources, for very extended sources such as NGC 1399, the extension and count rates given by the algorithm are underestimated. Moreover, when multiple observations are available we can improve the statistics by considering the full set of data. We have therefore recalculated all count rates, using the BMW – HRI positions and original HRI data retrieved from the public archives⁴, in pulse height analyzer (PHA) channels 1 – 10 to increase the signal-to-noise ratio (for a justification of this choice of PHA, see Trinchieri et al., 1997). When multiple observations of the same field are available, we summed the data if they have the same pointing coordinates and comparable exposure times. Otherwise, we typically used the longer exposures or those where the source is closer to the field’s center.

⁴ <http://wave.xray.mpe.mpg.de/>
<http://heasarc.gsfc.nasa.gov/>

3.1. Count rates

We classified sources as point-like or extended, based on the radial distribution of the emission relative to the shape of the HRI point spread function (PSF; for a description of the *ROSAT* PSF see Boese, 2000) at the corresponding off-axis angle. For the “extended sources” the counts are taken from the largest region that contains source counts, generally a circle of radius reported in Table 1, evaluated from the radial profile. In few cases, given the particular shape of the source, we used ellipses to evaluate the counts; we give in Table 1 minor and major semiaxis. There are also a few extended sources for which ad hoc regions (neither circles nor ellipses) have been used to estimate counts: these are PGC 5323, PGC 5324, PGC 13418, PGC 13433 and PGC 56962.

For point-like sources the counts are obtained in a circular region centered at the peak of X-ray emission, with radius that includes about 90% of source counts according to the PSF. The PSF degrades as the angular distance from the center of field increases, so we chose a radius of $r = 18''$ for $3' < \theta \leq 10'$, $r = 25''$ for $10' < \theta \leq 15'$ and $r = 40''$ for $\theta > 15'$, following Boese (2000). We evaluated the background in an annulus concentric to the source radius, with radii depending on the off-axis. When the source was particularly faint, we calculated count rates in a circle of radius corresponding to a smaller fraction of the PSF, to increase the signal-to-noise ratio. We then corrected the count rate accordingly, following Boese (2000).

We compared count rates obtained in this way with those reported in the BMW – HRI catalogue and we found a general agreement, with the exception of some sources whose extension had been largely underestimated by the wavelet algorithm, as stated above. Indeed, our count rates would be the equivalent to the “counted count rates” reported in the catalogue, rather than those computed with the wavelet algorithm. In the comparison with this quantity we found a systematically higher count rate, consistent with the larger PHA interval used (1 – 10 in our analysis and 2 – 9 in the BMW – HRI catalogue).

The resulting net count rates are given in Table 1, corrected for vignetting and lost counts due to the PSF (for point sources only).

3.2. Fluxes and luminosities

The count rates were converted into 0.1 – 2 keV fluxes using a conversion factor corresponding to a bremsstrahlung spectrum with $kT = 5$ keV plus the line of sight absorption appropriate for each source from Dickey & Lockman (1990) (reported in Table 2). Although this spectrum might not be suitable for all kinds of sources, the flux in the *ROSAT* energy window depends only weakly on the spectral model assumed, while it is more dependent on low energy absorption. The resulting fluxes are in the range $10^{-14} – 10^{-11}$ erg cm $^{-2}$ s $^{-1}$.

N_{H} (cm $^{-2}$)	CF (erg cm $^{-2}$ count $^{-1}$)
1×10^{20}	3.7×10^{-11}
2×10^{20}	4.1×10^{-11}
5×10^{20}	4.9×10^{-11}
8×10^{20}	5.5×10^{-11}
3×10^{21}	9.3×10^{-11}

Table 2. Galactic N_{H} and corresponding unabsorbed flux in the band 0.1 - 2 keV for 1 count/s, assuming a thermal bremsstrahlung spectral model with $kT = 5$ keV.

To calculate luminosities, we used distances listed in Table 1. The corresponding range in L_X is $10^{38} - 10^{43}$ erg s $^{-1}$.

4. The atlas

We provide in Fig. 2 an overlay of X-ray contours of the detected galaxies onto optical images from the Digital Sky Survey II (DSS II) available from the ESO archive⁵. The Figure is available in electronic edition. We report here the first page as an example. When available, we used optical images obtained with the blue filter, otherwise we used those obtained in the red filter. For PGC 209730 only the DSS I plate is available.

Galaxies, ordered in RA and generally at the center of the field, are identified by their PGC name.

X-ray contours are produced from images in the PHA range 1 – 10, smoothed with a Gaussian function with $\sigma = 5''$ for point-like sources and with $\sigma = 10''$ for extended sources.

5. Optical observations

In order to measure redshifts and magnitudes for some of the galaxies of our sample, we made spectroscopical and photometrical observations at the 1.52 meter telescope of the Osservatorio Astronomico di Bologna, at Loiano (Italy) on the nights of the 16th and 17th October 2001. Because of bad atmospheric conditions, we were able to observe only 3 galaxies. A spectrophotometric calibration star was also observed. We present the results obtained in Appendix A.

6. Comparison with literature results

To verify whether the total sample of 143 objects is representative of the X-ray properties of normal galaxies, we calculated X-ray luminosities where possible (Table 1) and we plotted the distributions of L_X , L_B , the ratio L_X/L_B and the L_X - L_B relationship for spiral and early-type galaxies. For the 19 galaxies for which the redshift is not known but we have m_B , the ratio is calculated from

⁵ <http://archive.eso.org/dss/dss>

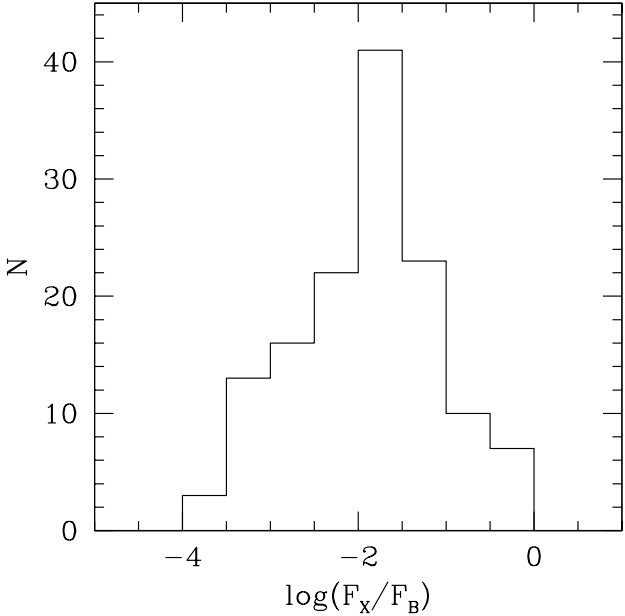


Fig. 3. X-ray - to - optical ratio distribution for the total sample. Both fluxes are in units of erg cm $^{-2}$ s $^{-1}$.

fluxes. We compared our results with those in the literature and found a good general agreement.

In particular:

1. the bulk of the galaxies in the sample has an X-ray luminosity between 10^{38} erg s $^{-1}$ and few 10^{42} erg s $^{-1}$, in accordance with, e.g., Fabbiano (1989); 7 objects have $L_X \gtrsim 10^{43}$ erg s $^{-1}$, but most of them lie in a group, so that the intergalactic medium could contribute to their luminosity; we cannot exclude the presence of an unidentified AGN for some of these objects.
2. For spiral galaxies we found a linear relationship between X-ray and optical luminosities ($L_X \propto L_B^{1.0 \pm 0.2}$), in agreement with Fabbiano et al. (1992). In a subsequent, more complete statistical analysis of the 234 “normal” spiral and irregular galaxies reported by Fabbiano et al. (1992), Shapley et al. (2001) and Fabbiano & Shapley (2002) find however that the $L_X - L_B$ relationship is significantly steeper than linear, with a slope of about 1.5. Our study is based on a much smaller sample (32 spiral and irregular galaxies), and small statistics could account for the discrepancy, as pointed out by Fabbiano & Shapley (2002) in comparing their findings with previous works.
3. For early-type galaxies we found a steeper relationship, $L_X \propto L_B^{1.6 \pm 0.2}$, consistent with those obtained by Fabbiano et al. (1992) and Eskridge et al. (1995).
4. Values of the X-ray - to optical ratio in our sample cover roughly the same range ($-4 < \log(L_X/L_B) < 0$ with L_X and L_B in erg s $^{-1}$) as the spiral galaxies in Shapley et al. (2001) and the early-type galaxies in Eskridge et al. (1995), but their distributions are different. We plot in Fig. 3 the histogram of the X-ray - to

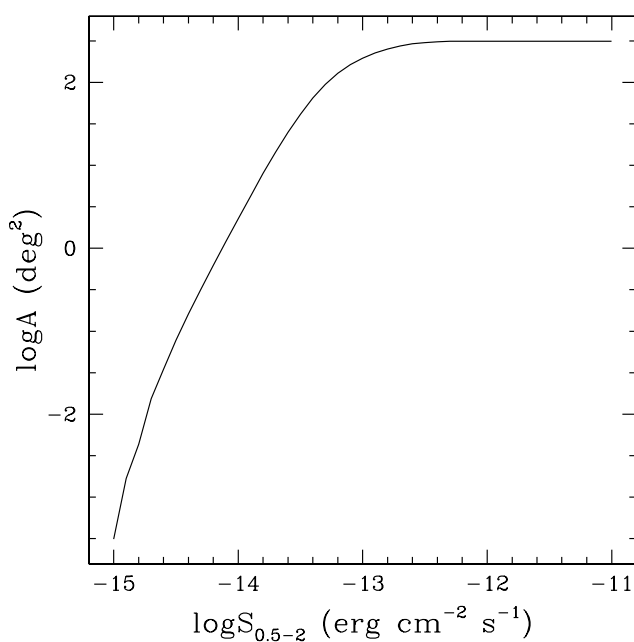


Fig. 4. Sky coverage for the fields at galactic latitude $|b| \geq 10^\circ$ and off-axis angle $3' \leq \theta \leq 18'$, computed by assuming a thermal bremsstrahlung spectrum with $kT = 5$ keV and galactic line of sight absorption.

- optical ratio of the total sample of 143 galaxies. We will analyze this subject in greater detail in subsection 7.1.

7. The logN-logS distribution

The complete serendipitous sample of galaxies derived in section 2.1 (listed in Table 3) was used to calculate the integral flux distribution (logN-logS) of normal galaxies with X-ray emission above the X-ray flux limit of the BMW – HRI Catalogue and B - magnitude ≤ 15.5 .

The sensitivity of the HRI instrument is not uniform over the entire field of view. Moreover the observing time is different for different fields so we need to calculate the area surveyed at any given flux (sky coverage).

In the BMW – HRI catalogue the published sky coverage was calculated by means of simulations (see Panzera et al., 2003). In this work we used a sky coverage calculated with the same procedure, but with parameters that reflect our source selection criteria. Therefore we included only fields with galactic latitude $|b| \geq 10^\circ$, we considered only an annular region with $3' \leq \theta \leq 18'$ (the lower limit is to account for the target region; the upper limit is the largest radius within the field of view of the detector in the assumption of circular symmetry) and we assumed a bremsstrahlung spectrum with $kT = 5$ keV plus the line of sight absorption.

The resulting sky coverage is plotted in Fig. 4. The maximum area is ~ 314 deg 2 and corresponds to fluxes above $\sim 10^{-12}$ erg cm $^{-2}$ s $^{-1}$. The surveyed area is ~ 196 deg 2 at 10^{-13} erg cm $^{-2}$ s $^{-1}$ and ~ 3 deg 2 at $\sim 1.1 \times$

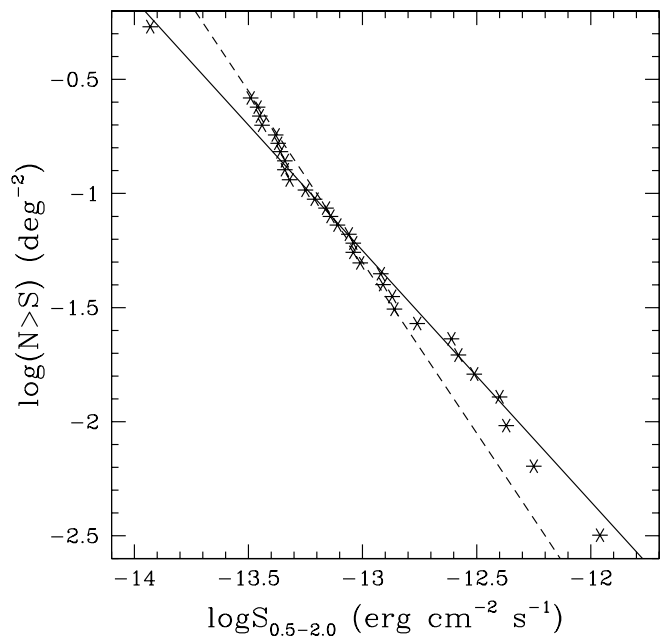


Fig. 5. The integral logN-logS distribution for the complete serendipitous subsample (asterisks); the solid line represents the -1.1 slope and the dashed line the euclidean -1.5 slope.

10^{-14} erg cm $^{-2}$ s $^{-1}$ (the lowest flux for the galaxies in our sample).

For consistency with the sky coverage calculation, the fluxes given in Table 3 are derived from the original count rates estimated in the BMW – HRI catalogue using the wavelet algorithm and PHA channels of HRI from 2 to 9, which are corrected for vignetting and PSF according to Campana et al. (1999) and computed for the energy band $0.5 – 2$ keV, the standard of BMW – HRI Catalogue.

The integral logN-logS distribution of the sample is shown in Fig. 5 and covers two decades in flux, from ~ 1.1 to $\sim 110 \times 10^{-14}$ erg cm $^{-2}$ s $^{-1}$. The overall distribution could be approximated with a slope of ~ -1.1 (solid line in Fig. 5). However the euclidean slope of -1.5 (dashed line) is also consistent with the data: the excess of galaxies at the highest fluxes is small and consistent within the limited statistics. Moreover, at the lower fluxes, we could have some problems with incompleteness, as we discuss below.

7.1. Comparison with the literature: X-ray - to - optical ratio distribution

Before comparing our logN-logS distribution with those of other samples in the literature, we need to better investigate the X-ray - to - optical ratio distribution of our complete sample. We will consider samples derived from *ROSAT* and *Einstein* observations that cover a flux range similar to ours. We will include samples derived from *XMM - Newton* and *Chandra* surveys, that cover a flux

LEDA name	N_H (10^{20} cm $^{-2}$)	Count rate (10^{-3} count s $^{-1}$)		F $_{0.5-2}$ (10^{-13} erg cm $^{-2}$ s $^{-1}$)	
0157406	4.9	0.37	\pm 0.07	0.12	\pm 0.02
0068536	2.5	1.11	\pm 0.34	0.32	\pm 0.09
0025825	4.2	1.12	\pm 0.22	0.35	\pm 0.06
0042833	2.0	1.31	\pm 0.23	0.35	\pm 0.05
0028990	0.8	1.50	\pm 0.30	0.36	\pm 0.07
0005323	3.8	1.33	\pm 0.28	0.41	\pm 0.09
0010446	3.1	1.48	\pm 0.24	0.43	\pm 0.06
0057078	2.3	1.63	\pm 0.28	0.44	\pm 0.08
0069338	8.8	1.24	\pm 0.20	0.46	\pm 0.07
0038773	2.0	1.70	\pm 0.11	0.46	\pm 0.03
0001333	4.2	1.55	\pm 0.27	0.48	\pm 0.09
0007289	5.5	1.71	\pm 0.26	0.56	\pm 0.10
0070861	2.6	2.11	\pm 0.38	0.61	\pm 0.12
0018991	5.4	2.18	\pm 0.32	0.70	\pm 0.10
0004117	4.0	2.36	\pm 0.23	0.73	\pm 0.06
0043675	3.9	2.49	\pm 0.37	0.77	\pm 0.12
0002204	1.9	3.23	\pm 0.23	0.87	\pm 0.05
0045318	1.0	3.78	\pm 0.60	0.91	\pm 0.14
0046432	3.2	3.13	\pm 0.66	0.91	\pm 0.20
0047432	2.3	3.61	\pm 0.64	0.97	\pm 0.16
0130966	2.4	4.41	\pm 0.81	1.19	\pm 0.22
0016574	5.9	3.73	\pm 0.51	1.23	\pm 0.17
0005324	3.8	4.34	\pm 0.51	1.35	\pm 0.16
0057728	1.5	5.11	\pm 0.39	1.38	\pm 0.11
0013368	1.4	7.22	\pm 1.41	1.73	\pm 0.24
0029050	0.8	10.20	\pm 0.70	2.45	\pm 0.17
0002362	2.7	9.06	\pm 0.99	2.63	\pm 0.29
0004848	6.1	9.26	\pm 2.43	3.06	\pm 0.66
0063122	7.9	11.02	\pm 1.42	3.97	\pm 0.36
0006367	3.0	14.80	\pm 0.60	4.29	\pm 0.17
0017451	7.5	15.66	\pm 1.72	5.64	\pm 0.72
0028995	4.8	34.20	\pm 2.00	10.94	\pm 0.64

Table 3. Galactic column density (from Dickey & Lockman 1990), BMW count rates and fluxes for galaxies in the complete serendipitous sample, ordered by increasing flux.

range significantly fainter than ours, in the discussion of the logN-logS (subsection 7.2).

The best available comparison could be with the sample of *candidate normal galaxies* found by Zimmermann et al. (2001) in the *ROSAT* All Sky Survey (RASS) and with the normal galaxies found in the Einstein Extended Medium Sensitivity Survey (EMSS; Gioia et al., 1990), both X-ray selected. An effectively optically selected sample for comparison is the *Einstein* galaxy sample (Fabbiano et al., 1992; Shapley et al., 2001; Eskridge et al., 1995).

Zimmermann et al. (2001) made a correlation study of the RASS Bright Source Catalogue (Voges et al., 1999) with the Catalogue of Principal Galaxies (Paturel et al., 1989), from which they selected a sample of 198 *candidate galaxies*, i.e. X-ray sources whose optical counterpart was not designated as AGN in the literature. These selection criteria are similar to ours, and the Catalogue of Principal Galaxies is a preliminary version of the current LEDA database, so the two samples can be easily compared; how-

ever most of the Zimmermann et al. (2001) sources have fluxes above 10^{-12} erg cm $^{-2}$ s $^{-1}$ (computed in the 0.1–2.4 keV band, assuming a power law spectrum with photon index $\Gamma = 2.3$).

The EMSS was obtained from the analysis of 1453 images of the imaging proportional counter (IPC) on board the *Einstein* Observatory. The survey covers an area of 778 deg 2 at $|b| > 20^\circ$ with limiting sensitivity ranging from $\sim 5 \times 10^{-14}$ to $\sim 3 \times 10^{-12}$ erg cm $^{-2}$ s $^{-1}$ (0.3–3.5 keV band). 835 serendipitous sources were detected at or above the 4 σ level (see Gioia et al., 1990; Stocke et al., 1991). Among these, 17 were identified as normal galaxies.

The *Einstein* sample is the catalogue of normal galaxies observed by the *Einstein* satellite, compiled by Fabbiano et al. (1992) and reanalyzed by Eskridge et al. (1995, for early-type galaxies) and by Shapley et al. (2001, for spiral galaxies); we no longer distinguish here the two samples since early and late type galaxies are mixed in the BMW – HRI sample.

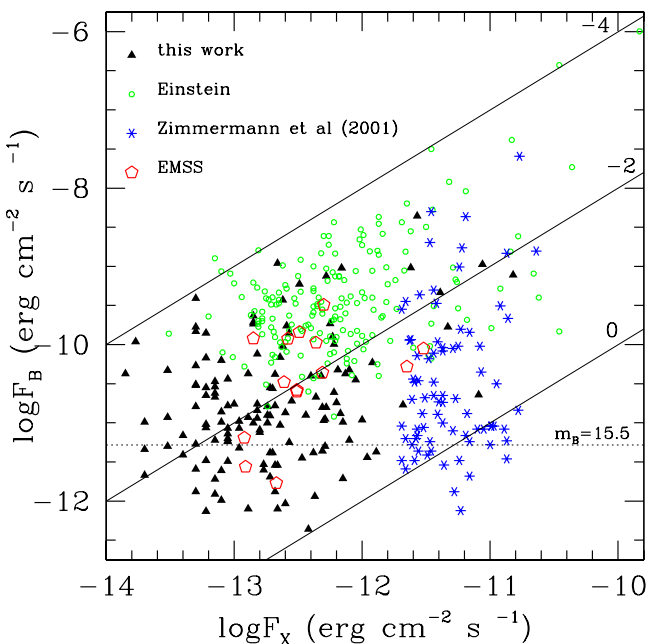


Fig. 6. B flux versus X-ray flux for our total sample (solid triangles), for the *Einstein* sample (empty circles), for the Zimmermann et al. 2001 sample galaxies (asterisks), and for the EMSS galaxies (empty pentagons). Solid lines correspond to $\log(F_X/F_B) = 0, -2, -4$, as indicated; the horizontal dashed line is the $m_B = 15.5$ limit. We have considered only detections in the *Einstein* sample: the exclusion of upper limits should not affect the results, since their distribution is consistent with that of the detections (see Fig. 5 in Shapley et al. 2001). We do not plot objects at $F_{0.1-2} < 2 \times 10^{-12}$ erg cm $^{-2}$ s $^{-1}$ in the Zimmermann et al. (2001) sample because below this flux their sample is not complete (see text).

In Fig. 6 we plot the distribution of F_X and F_B values from all samples considered. For consistency with the values in Table 1, all fluxes are converted to the 0.1 – 2 keV energy band, using a thermal bremsstrahlung spectrum with temperature $kT = 5$ keV and $N_H = 3 \times 10^{20}$ cm $^{-2}$.

Fig. 6 clearly indicates that galaxies belonging to different samples populate different regions in the plot. Our sample (solid triangles) has an X-ray flux range between 10^{-14} and 10^{-11} erg cm $^{-2}$ s $^{-1}$ and $\log(F_X/F_B)$ between -4 and 0 (see also Fig. 3). The bulk of *Einstein* galaxies (empty circles) is typically at higher average fluxes and at lower values of $\log(F_X/F_B)$ (between -4 and -2) compared to our distribution and the X-ray selected samples in general. This sample is the largest, it is effectively optically selected and reasonably clean of the contamination from AGN (Shapley et al., 2001). However, since it is not complete, it might not provide the true distribution of the X-ray - to - optical ratios.

The second largest sample is derived from Zimmermann et al. (2001), with an additional flux limit $F_X > 2 \times 10^{-12}$ erg cm $^{-2}$ s $^{-1}$ (for completeness,

see discussion below) and an upper limit in luminosity at $\log L_X = 42.7$ erg s $^{-1}$ (the highest luminosity in our complete sample), comparable to their limit to exclude potential AGNs from the sample. The distribution of *candidate galaxies* of Zimmermann et al. (2001) (asterisks) is significantly different from that of the *Einstein* sample and extends at $\log(F_X/F_B) > 0$.

The F_X/F_B distribution for EMSS galaxies (empty pentagons) is at intermediate values and more consistent with that of our sample.

Also plotted in Fig. 6 is the optical flux limit applied to our sample, $m_B = 15.5$. It is evident that the exclusion of galaxies fainter than this for the logN-logS calculation has an effect that increases as flux decreases. We have attempted to quantify it in order to correct the curve for lost objects. Unfortunately we could not properly estimate the correction because none of the galaxy samples available allows us to derive the true distribution of X-ray - to - optical ratios of normal galaxies. The EMSS should represent the true F_X/F_B distribution, but, given the small number of galaxies (17, of which only 15 with B-magnitude), statistical errors are large. The difference in the distribution of ratios between the two larger samples in Fig. 6 suggests that they might be affected by opposite biases: the Zimmermann et al. (2001) sample is likely to contain unclassified AGNs, while the *Einstein* sample could lose objects at the highest X-ray - to - optical ratios. If we use the three samples to estimate how many galaxies are lost as a function of X-ray flux, we find that the corrections to the logN-logS are small and the recomputed curve is consistent with the euclidean slope in the observed flux range.

We also tried to estimate the correction by considering optically fainter galaxies. At $m_B = 16$, LEDA is about 90% complete (see Fig. 7 in Paturel et al., 1997): if we include galaxies down to this flux limit, we only add 4 objects to our serendipitous sample, distributed over the whole range of X-ray fluxes. Their inclusion only has a marginal influence on the normalization, and none on the slope of the distribution.

We conclude that, since the effects introduced by the optical limit are small, the logN-logS we derive is consistent with the euclidean slope.

7.2. Comparison with the literature: logN-logS

Figure 7 shows the comparison between the logN-logS derived above with several available from the literature. All fluxes are recomputed in the 0.5 – 2 keV range that we use.

We find an excellent agreement with other samples that cover similar or brighter flux ranges than the present sample.

The *candidate galaxies* (Zimmermann et al., 2001) appear to connect smoothly with the euclidean extrapolation of the BMW – HRI logN-logS above 10^{-12} erg cm $^{-2}$ s $^{-1}$. We interpret the flattening observed in the

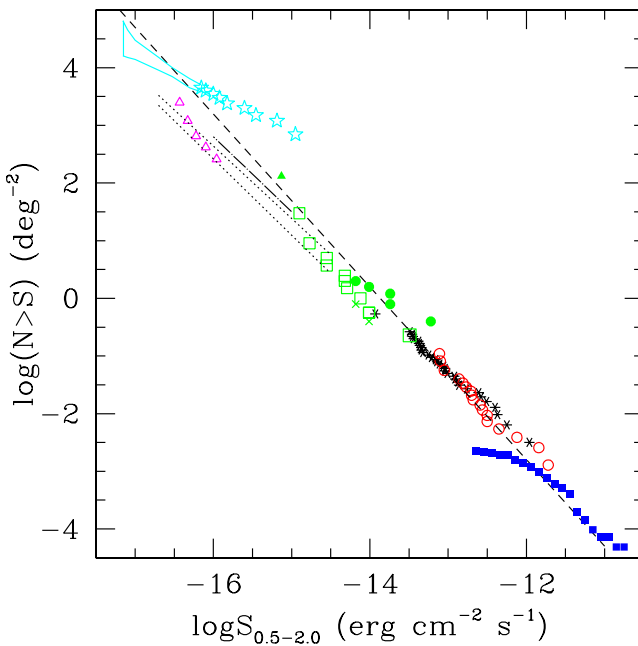


Fig. 7. Comparison of the logN-logs distribution obtained from the present sample (asterisks) with several other relations for normal galaxies from the literature. The dashed line represents the Euclidean relationship of Figure 5 extrapolated to the full flux range considered. Symbols refer to: EMSS galaxies (empty circles); *candidate galaxies* in Zimmermann et al. 2001 (solid squares); normal galaxies (crosses), including LLAGN (solid circles) (Georgakakis et al. 2004a), and stacking analysis (solid triangles, Georgakakis et al. 2003), found in the *XMM-Newton*/2dF survey; *XMM-Newton*/Sloan DSS normal galaxies from Georgakakis et al. (2004b) (empty squares); *Chandra* Deep Fields results from Hornschemeier et al. (2003) (empty triangles); optimistic or pessimistic curves given by Bauer et al. (2004) (upper/lower dotted line); Bayesian sample of Norman et al. (2004) reported by Ranalli et al. (2004) (dot-dashed line). Open stars and horned-shaped box indicate the detections and fluctuation analysis predictions of Miyaji & Griffiths (2002).

Zimmermann et al. (2001) data at lower fluxes as a result of their selection criteria. In fact, they indicate a $\geq 90\%$ completeness for count rates ≥ 0.1 count s^{-1} , which converts to a flux of $F_{0.5-2} \sim 7 \times 10^{-13}$ erg $cm^{-2} s^{-1}$.

Although small, the EMSS is a truly complete sample, since it is serendipitously X-ray selected and virtually completely identified (Gioia et al., 1990; Stocke et al., 1991; Maccacaro et al., 1994). The EMSS appears to be Euclidean and almost coincident with our curve for fluxes above 10^{-13} erg $cm^{-2} s^{-1}$.

We have also extended the comparison to include samples at fainter fluxes. Georgakakis et al. (2004a) have computed the logN-logS of sources in the XMM - Newton/2dF survey, obtained with the EPIC instrument on board the *XMM-Newton* satellite. This survey covers an area of about 2.5 deg 2 to the flux limit $\sim 10^{-14}$ erg

cm $^{-2} s^{-1}$ in the $0.5 - 8$ keV band (or $F_{0.5-2} \sim 5 \times 10^{-15}$ erg $cm^{-2} s^{-1}$). They find two “normal” galaxies in their sample, that imply a density of < 1 source at $F_X \sim 10^{-14}$ erg $cm^{-2} s^{-1}$, lower than what we find.

However, the sample of Georgakakis et al. (2004a) contains three additional galaxies (at $z \leq 0.1$ with $L_{0.5-8} \sim 10^{42}$ erg s^{-1}) that the authors do not consider because they might contain Low Luminosity AGNs (LLAGNs, see their Fig. 2). Since we cannot exclude that our sample also contains a few LLAGNs (see above and section 6), we should consider these objects for a better comparison with our sample. With the inclusion of these objects the logN-logS better matches ours.

Also shown in Fig. 7 are the constraints from the stacking analysis results of Georgakakis et al. (2003) at fainter fluxes, computed from optically selected galaxies at a mean redshift of $z \sim 0.1$. The point derived from the total sample considered is in excellent agreement with our logN-logS.

Recently Georgakakis et al. (2004b) have presented a pilot sample of normal galaxies serendipitously detected in *XMM-Newton* public observations. They found 11 “normal” galaxy candidates with luminosities below 10^{42} erg s^{-1} over an area of ~ 4.5 deg 2 . They find that the LogN-LogS derived from this sample (plotted in Fig. 7) is again almost Euclidean in slope, although at a smaller normalization than ours.

We also plot the results from deeper surveys, using data from Hornschemeier et al. (2003), Norman et al. (2004) as reported by Ranalli et al. (2004), Bauer et al. (2004), derived from the *Chandra* Deep Fields. All these relations fall close to, although in general below, the extrapolation from our sample. Different authors derive different slopes for their samples, but they are all consistent with the Euclidean one.

The lower normalizations found in these latter samples could be explained in part by the combined effects of more stringent criteria to minimize contamination from the AGNs, even though of low luminosity, and of different relative occurrence of the galaxy types (spiral/starburst vs early types).

As already discussed, some residual contamination from low luminosity AGNs could be present in the sample we have considered, since we have little information on the optical spectra, and could only reject known AGNs. We note however that Zimmermann et al. (2001) have applied the same criterium adopted by Georgakakis et al. (2004a), namely an X-ray to optical luminosity ratio smaller than 10^{-2} , and that the EMSS sample, which is well studied optically, should not be contaminated by AGNs. We have nevertheless considered discarding sources in our sample that have a $\log(F_{0.5-2}/F_B) < -2$. We have 7 objects that violate this limit, mostly at the high flux end. The resulting logN-logS relation is slightly steeper, but consistent with that presented in Fig. 5, and would not significantly lower the normalization of the “Euclidean” curve plotted. However the location of the different points from Georgakakis et al. (2004a) that consider/discard possible

contamination from LLAGNs give an idea of the possible uncertainties involved.

The effect of different relative contributions from the early/late types is more complicated to assess. The lowest flux points (Hornschemeier et al., 2003) are derived from late type galaxies, so they could underrepresent the total population. However, Bauer et al. (2004) suggest that the early type galaxies follow a flatter distribution, and in any case their LogN-logS is always below those from starburst/quiescent galaxies (see their Fig. 9), so their contribution could in fact be negligible at the fainter fluxes. In the range covered by Georgakakis et al. (2004b), there is only one early type galaxy (but the sample is very small), while in our sample we have a sizeable fraction of early types (1/3 among the objects with a morphological classification), and the percentage increases to $\sim 50\%$ in the “candidate normal galaxies” of Zimmermann et al. (2001), for which moreover there is no apparent significant difference in the two slopes either. The stacking analysis results from Georgakakis et al. (2003) derived separately for E/S0 and Sa-Scd bracket the extrapolation of the euclidean logN-logS obtained from brighter samples, with Sa-Scd in better agreement with the samples at low fluxes. Since the emission from early and late type galaxies is due to significantly different processes (Fabbiano, 1989; Fabbiano et al., 1992; Kim et al., 1992; Eskridge et al., 1995; Shapley et al., 2001), a different evolution is not out of the question. An assessment of the local LogN-logS separately for the different morphological types would be a step forward to a better understanding of the properties of galaxies as a class, and would provide stronger constraints for the investigation of normal galaxies at higher redshifts. Investigating this aspect is beyond the scope and the potential of this work. For the present time, we simply notice how remarkable it is that, in spite of the different selection criteria and instruments used to define all the samples considered, the surface densities of normal galaxies is consistent with a single euclidean distribution for about 6 decades in flux (from $\sim 10^{-11}$ to $\sim 3 \times 10^{-17}$ erg $\text{cm}^{-2} \text{ s}^{-1}$).

8. Conclusions

We present the results for an “almost serendipitous” sample of 143 X-ray emitting normal galaxies selected from the cross-correlation of the BMW – HRI Catalogue and the LEDA database. Isointensity X-ray contours are overlayed onto the optical images for all galaxies and are presented in an atlas in Fig. 2. The X-ray characteristics of the sample, listed in Table 1, are derived in a uniform way and are used in comparison with other samples in the literature. We find that the general properties of the total sample are in good agreement with those already known for normal galaxies.

We have also selected a complete subsample of 32 truly serendipitous sources in the local universe ($z < 0.07$), for which we derived the logN-logS distribution in the flux range between ~ 1.1 and 110×10^{-14} erg $\text{cm}^{-2} \text{ s}^{-1}$, in

the 0.5 – 2 keV energy band. We find that the relation is consistent with the euclidean distribution.

Moreover, we find a good agreement between our logN-logS and those derived from *ROSAT* PSPC and *Einstein* data at similar or brighter fluxes and from *XMM - Newton* and *Chandra* at fainter fluxes: the overall distribution appears to be consistent with an euclidean slope for about 6 decades in flux, from $\sim 3 \times 10^{-17}$ to 10^{-11} erg $\text{cm}^{-2} \text{ s}^{-1}$. The normalizations of different samples are consistent within a factor of ~ 2 .

Although with limited statistics, this work provides a first estimate of the number density of sources identified with normal galaxies in the nearby universe, in a flux range (both optical and X-ray) easily accessible for follow up detailed observations. This will allow us to provide a solid basis that will help in studying and classifying objects found in deeper surveys.

While current efforts are mainly focused on probing the distant universe to determine the relevance of normal galaxies as a class at very faint fluxes, the success of these studies depends also on the constraints given by the bright flux end of the number counts, which is still poorly studied. This is particularly relevant at the lowest fluxes where the number counts approach the total source density (e.g. the detections and fluctuation analysis results of Miyaji & Griffiths (2002), see Hornschemeier et al. (2002) and Fig. 7). The sample here derived will be therefore instrumental to studies of both the galaxy cosmological evolution and the contribution of this class of sources to the X-ray background.

Acknowledgements. We thank Dr. R. Panzera for her invaluable help, in particular in the extraction of our sample from the BMW – HRI catalogue.

We thank Dr. U. Zimmermann for useful discussion on their work and for providing us with the original data for their logN-logS that we use in Fig. 7.

We acknowledge partial financial support from the Italian Space Agency (ASI).

This research has made use of the Lyon-Meudon Extragalactic Database (LEDA), <http://www-obs.univ-lyon1.fr/hypercat/> or <http://www.brera.mi.astro.it/hypercat/>.

This research has made use of the NASA/IPAC Extragalactic Database (NED) which is operated by the Jet Propulsion Laboratory, California Institute of Technology, under contract with the National Aeronautics and Space Administration.

This research has made use of the SAOImage ds9 developed by the Smithsonian Astrophysical Observatory.

The compressed files of the “Palomar Observatory - Space Telescope Science Institute Digital Sky Survey” of the northern sky, based on scans of the Second Palomar Sky Survey are copyright (c) 1993-2000 by the California Institute of Technology and are distributed by agreement. All Rights Reserved.

References

Bauer, F. E., Alexander, D. M., Brandt, W. N. et al., 2004, accepted for publication in AJ, astro-ph/0408001

Beuing, J., Döbereiner, S., Böhringer, H. & Bender, R. 1999, MNRAS 302, 209

Boese, F. G. 2000, A&AS 141, 507

Brandt, W. N., Hornschemeier, A. E., Alexander, D. M., et al. 2001, AJ 122, 1

Brown, B. A. & Bregman, J. N. 1998, ApJ 495L, 75

Campana, S., Lazzati, D., Panzera, M. R. & Tagliaferri, G. 1999, ApJ 524, 423

David, L. P., Jones, C. & Forman, W., 1992, ApJ 388, 82

Dell'Antonio, I. P., Geller, M. J. & Fabricant, D. G. 1994, AJ 107 427

Dickey, J. M. & Lockman, F. J. 1990, ARA&A 28, 215

Eskridge, P. B., Fabbiano, G. & Kim, D.-W. 1995, ApJS 97, 141

Fabbiano, G. 1989, ARA&A 27, 87

Fabbiano, G. & Shapley, A., 2002, ApJ 565, 908

Fabbiano, G. & Trinchieri, G. 1987, ApJ 315, 46

Fabbiano, G., Kim, D.-W. & Trinchieri, G. 1992, ApJS 80, 531

Georgakakis, A., Georgantopoulos, I., Stewart, G. C., Shanks, T., & Boyle, B. J. 2003, MNRAS 344, 161

Georgakakis, A., Georgantopoulos, I., Vallbe, M., et al. 2004a, MNRAS 349, 135

Georgakakis, A., Georgantopoulos, I., Basilakos, S., Plionis, M. & Kolokotronis, V., 2004b, MNRAS in press, astro-ph/0407387

Gioia, I. M., Maccacaro, T., Schild, R. E., et al. 1990, ApJS 72, 567

Helsdon, S. F. & Ponman, T. J. 2000, MNRAS 319, 933

Helsdon, S. F. & Ponman, T. J. 2003, MNRAS 340, 485

Hornschemeier, A. E., Bauer, F. E., Alexander, D. M., et al. 2003, AJ 126, 575

Hornschemeier, A. E., Brandt, W. N., Alexander, D. M., et al. 2002, ApJ, 568, 82

Jones, L. R., Ponman, T. J., Horton, A., et al. 2003, MNRAS 343, 627

Kim, D.-W., Fabbiano, G., & Trinchieri, G. 1992, ApJS, 80, 645

Lazzati, D., Campana, S., Rosati, P., Panzera, M. R. & Tagliaferri, G. 1999, ApJ 524, 414

Maccacaro, T., Gioia, I. M., Wolter, A., Zamorani, G. & Stocke, J. T. 1988, ApJ 326, 68

Maccacaro, T., Wolter, A., McLean, B., et al. 1994, ApL&C 29, 267

Mahdavi, A., Böhringer, H., Geller, M. J. & Ramella, M. 1997, ApJ 483, 68

Mamon, G. A. 1992, in *Physics of Nearby Galaxies: Nature or Nurture?*, ed T. X. Thuan, C. Balkowski & J. Tran Thanh Van (Gif-sur-Yvette:Editions Frontières), 367

Miyaji, T. & Griffiths, R. E., 2002 ApJ 564L, 5

Mulchaey, J. S. & Zabludoff, A. I. 1998, ApJ 496, 73

Mulchaey, J. S., Davis, D. S., Mushotzky, R. F. & Burstein, D., 2003, ApJS 145, 39

Norman, C., Ptak, A., Hornschemeier, A., et al. 2004, ApJ 607, 721

Osmond, J. P. F. & Ponman, T. J., 2004, MNRAS 350, 1511

Panzera, M. R., Campana, S., Covino, S., et al. 2003, A&A 399, 351

Paturel, G., Andernach, H., Bottinelli, L., et al. 1997, A&AS 124, 109

Paturel, G., Fouqué, P., Bottinelli, L. & Gouguenheim, L. 1989, A&AS 80 299

Pildis, R. A., Bregman, J. N. & Evrard, A. E. 1995, ApJ 443, 514

Ponman, T. J., Bourner, P. D. J., Ebeling, H., & Böhringer, H. 1996, MNRAS 283, 690

Ranalli, P., Comastri, A. & Setti, G., proc. conf. *Multiwavelength AGN Surveys*, Cozumel, Mexico 2003, astro-ph/0404087

Read, A. M., Ponman, T. J. & Strickland, D. K. 1997, MNRAS 286, 626

Roberts, T. P. & Warwick, R. S. 2000, MNRAS 315, 98

Sandage, A. & Tammann, G. A., *Revised Shapley-Ames Catalog of Bright Galaxies* 1981, Carnegie Inst. of Washington, Publ. 635

Severgnini, P., Caccianiga, A., Braito, V., et al. 2003, A&A, 406, 483

Shapley, A., Fabbiano, G. & Eskridge, P. B. 2001, ApJS 137, 139

Stocke, J. T., Morris, S. L., Gioia, I. M., et al. 1991, ApJS 76, 813

Trinchieri, G., Noris, L. & di Serego Alighieri, S., 1997, A&A 326, 565

Trinchieri, G., Fabbiano, G. & Peres, G. 1988, ApJ 325, 531

Tully, R. B., *Nearby galaxies catalog*, Cambridge and New York, Cambridge University Press, 1988

de Vaucouleurs, G., de Vaucouleurs, A. & Corwin, J. R., *Second reference catalogue of bright galaxies* 1976, Austin: University of Texas Press

Véron-Cetty, M.-P. & Véron, P., 2001, A&A 374, 92

Voges, W., Aschenbach, B., Boller, T., et al. 1999, A&A 349, 389

Vogler, A. & Pietsch, W. 1996, A&A, 311, 35

White, N. E., Giommi, P., & Angelini, L. 1994, Bulletin of the American Astronomical Society, 26, 1372

Zimmermann, H.-U., Boller, T., Döbereiner, S. & Pietsch, W. 2001, A&A 378, 30

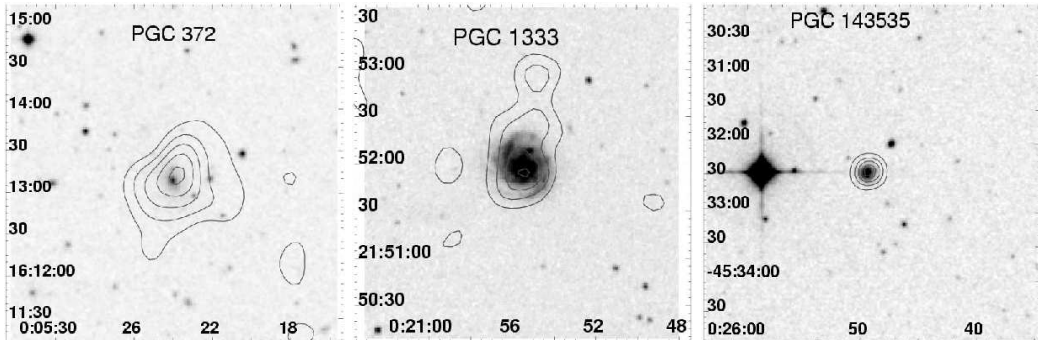


Fig. 2. First page of the figure available in electronic form, that presents the X-ray contours from smoothed X-ray images superimposed onto optical images. Galaxies are generally at the center of the field. Smoothing is done with a Gaussian function of $\sigma = 5''$ for point-like sources and of $\sigma = 10''$ for extended sources.

Appendix A: Results of optical observations

The log of observations made at the Loiano Telescope in order to measure redshifts and magnitudes for some galaxies in our sample (see section 5) is listed in Table A.1.

The seeing was about $2''$, so we used a long slit of width $2.5''$ for spectra. The spectral range was 3800 \AA - 8700 \AA .

For photometry we used the B - V - R filters of Johnson - Kron - Cousin system.

We made use of the Image Reduction and Analysis Facility (IRAF)⁶ for spectroscopic and photometric data reduction.

We used all lines visible in the spectra to measure z , which is calculated from the average value. The redshifts obtained are reported in Table A.2. Only absorption lines, typical of early-type galaxies, and no sign of nuclear activity were detected in the galaxy spectra.

The atmospheric conditions were inadequate for photometric observations, however we list our raw estimate of magnitudes in Table A.3 and we use the value obtained for PGC 69291 in Table 1, where it is reported in brackets.

PGC 196693

After obtaining the spectrum, we discovered that NED lists the galaxy SDSS J234817.99+010617.0 at the same position and with the same redshift we obtained, although it does not give a PGC name. We therefore identify PGC 196693 as SDSS J234817.99+010617.0.

PGC 69291

The galaxy is identified as NGC 7325 by LEDA and as NGC 7327 by NED, with a note suggesting that it could be a star. Our observations show 2 objects, a star and a galaxy at $z = 0.0290 \pm 0.0009$ at the position of PGC 69291. Most of the optical flux is due to the star, as listed in Table A.3.

The uncertainty in the X-ray position (see also the map in Fig. 2) does not allow us to identify the X-ray source with either object. Unfortunately the bad quality of our optical does not allow us to use the X-ray - to - optical ratio (see for example Maccacaro et al., 1988) to discriminate between them, because it is consistent with both the star and the galaxy. We list the galaxy in the total sample but due to its faint estimated magnitude it is not included in the complete serendipitous sample.

Appendix B: Table of total sample

We report here the complete table with our total sample that will be available in the electronic form. For explanation of the columns refer to the sample Table 1 in the main text.

⁶ IRAF is a general purpose software system for the reduction and analysis of astronomical data. IRAF is written and supported by the IRAF programming group at the National Optical Astronomy Observatories (NOAO) in Tucson, Arizona. NOAO is operated by the Association of Universities for Research in Astronomy (AURA), Inc. under cooperative agreement with the National Science Foundation.

Name	LEDA coordinates		Spectroscopy Exposure (s)	Photometry	
	R. A. (2000)	Dec. (2000)		Filter	Exposure (s)
PGC 65435	20 48 43.09	25 16 53.0	2 × 1800	R	2 × 120
PGC 69291	22 36 33.58	34 30 04.5	2 × 1800	R	1 × 60
				R	3 × 40
				V	1 × 40
				V	3 × 80
				B	3 × 200
PGC 196693	23 48 18.07	01 06 17.3	1 × 1800		
Feige 110	23 19 58.40	-05 09 56.2	2 × 480	R	2 × 30
				V	2 × 30
				B	2 × 40

Table A.1. Log of optical observations.

Name	Redshift
PGC 65435	0.0485 ± 0.0006
PGC 69291	0.0290 ± 0.0009
PGC 196693	0.093 ± 0.001

Table A.2. Average value of redshifts measured for the three galaxies observed.

Name	Magnitude		
	B	V	R
PGC 65435			14.8
PGC 69291 galaxy	16.6	16.1	15.6
PGC 69291 star	13.0	12.5	12.2

Table A.3. Estimated magnitudes for two of the three galaxies observed and for the star found near PGC 69291 resulting from our observations with the Loiano Telescope.

BMW042900.6-533653	04 29 00.91	-53 36 45.0	p	PGC 0015231	IC 2081	E-S0	255	14.62	3.39	0.60	1.25	0.22	41.98	C1
BMW042900.7-533647				PGC 0130376		E		15.53	12.38	2.04	5.08	0.84		
BMW043754.0-425852	04 37 55.01	-42 58 53.0	p	PGC 0099957		E	430	15.41	6.05	1.63	2.66	0.72	42.75	C1
BMW044707.0-202847	04 47 06.29	-20 28 39.2	p	PGC 0016574	NGC 1741	Sm	81	14.56	3.60	0.91	1.84	0.46	41.15	c; Gr
BMW050138.5-041527	05 01 38.26	-04 15 33.5	p	PGC 0147040		S0-a		17.00	0.89	0.34	0.49	0.19		
BMW050943.5-083652	05 09 44.01	-08 36 51.9	p	PGC 0017451	ESO 56-G154		145	13.42	16.17	1.94	8.90	1.07	42.33	c
BMW053359.9-714524	05 34 00.41	-71 45 28.5	p	PGC 0018991	UGC 3435		86	14.19	3.17	0.82	1.55	0.40	41.10	c
BMW062457.1+821914	06 24 57.12	+82 19 13.8	p	PGC 0075751	CGMW 1-0108	Sc			12.25	0.66	11.39	0.62		
BMW062545.7-042202	06 25 45.47	-04 22 04.4	p	PGC 0077028	CGMW 2-0778	Sbc		13.74	17.30	3.91	10.03	2.27		
BMW062545.8-042203				PGC 0021231	NGC 2300	E-S0	47	11.61	10.90	0.43	5.56	0.22	41.15	Gr
BMW071957.5-320041	07 19 58.78	-32 00 54.4	p	PGC 0078533	CGMW 1-1742	Sc			1.25	0.26	0.72	0.15		
BMW073217.8+854234	07 32 17.80	+85 42 34.1	e	PGC 0022928	CGCG 207-40		379	15.90	22.15	1.17	10.85	0.57	43.25	C1
BMW073220.2+854230				PGC 0023450			775	17.61	1.27	0.59	0.60	0.28	42.61	C1
BMW074914.6-055607	07 49 14.56	-05 56 11.3	p	PGC 0025701			958	17.27	1.69	0.26	0.82	0.13	42.92	C1
BMW081023.2+421628	08 10 23.16	+42 16 27.1	e	PGC 0025741			978	17.07	1.50	0.31	0.66	0.14	42.88	C1
BMW082133.8+470242	08 21 33.55	+47 02 37.7	p	PGC 0025825	NGC 2773	Sb	109	14.26	1.05	0.32	0.50	0.15	40.83	c
BMW090825.4-093349	09 08 25.49	-09 33 41.9	p	PGC 0025876	NGC 2777	Sab	26	14.45	1.67	0.31	0.79	0.15	39.79	Gr
BMW090825.7-093336				PGC 0087445			315	15.68	9.97	1.13	4.89	0.56	42.74	C1
BMW090851.5+110122	09 08 51.50	+11 01 22.0	e	PGC 0028995	ESO 567-G3	Sab		14.30	10.91	1.26	5.34	0.61		c; Gr?
BMW090852.1+110138				PGC 0028990	MCG 9-17-9		31	15.20	1.10	0.38	0.41	0.14	39.64	c; Gr
BMW090943.9+071032	09 09 43.87	+07 10 31.5	p	PGC 0029050	NGC 3079	SBcd	31	9.84	18.44	1.18	6.82	0.44	40.87	c; Gr
BMW091041.7+071223	09 10 41.86	+07 12 27.0	p	PGC 0029594	CGCG 266-27		261	15.38	2.57	1.27	0.95	0.47	41.84	
BMW091826.3-122222	09 18 27.00	-12 22 26.9	e	PGC 0030099	NGC 3193	E	35	11.72	1.21	0.31	0.50	0.13	39.84	Gr
BMW100108.4-192631	10 01 08.92	-19 26 26.8	p	PGC 0031453			215	14.71	9.12	2.81	4.47	1.38	42.42	C1
BMW100108.7-192621				PGC 0031540	NGC 3315	E-S0	75	13.84	1.39	0.36	0.68	0.18	40.65	C1
BMW100114.9+554316	10 01 15.17	+55 43 06.0	p	PGC 0032306	NGC 3389	Sc	34	11.63	3.23	0.89	1.42	0.39	40.26	Gr
BMW100115.1+554318				PGC 0032390	IC 2604	SBm	50	14.18	2.45	0.51	1.01	0.21	40.45	
BMW100115.5+554308				PGC 0033514	CGCG 213-27		170	15.92	9.06	2.70	3.35	1.00	42.05	
BMW100158.3+554100	10 01 58.60	+55 40 49.0	e	PGC 0035780	IC 711	E-S0	194	14.95	1.39	0.41	0.57	0.17	41.41	C1
BMW100158.3+554060				PGC 0035785	IC 712	E	201	13.67	1.48	0.45	0.61	0.18	41.44	C1
BMW100158.4+554103				PGC 0036348	NGC 3825	SBa	128	13.57	1.26	0.33	0.55	0.15	40.97	Gr
BMW100158.7+554051				PGC 0036369	MCG +10-17-46			15.82	1.21	0.32	0.45	0.12		
BMW101010.1+541828	10 10 10.10	+54 18 27.7	p	PGC 0139685			458	16.51	4.29	1.43	1.76	0.59	42.65	C1
BMW101825.0+215348	10 18 25.03	+21 53 45.9	e	PGC 0139725			815	17.55	3.24	0.57	1.33	0.23	42.99	
BMW103633.4-271318	10 36 33.36	-27 13 17.4	e	PGC 0038218	NGC 4077	S0	140	13.97	1.68	0.64	0.69	0.26	41.19	Gr
BMW103719.0-271121	10 37 18.92	-27 11 24.8	e	PGC 0157406				14.62	0.52	0.17	0.25	0.08		c
BMW104827.8+123157	10 48 27.76	+12 31 56.6	e	PGC 0038773	NGC 4156	SBb	135	13.65	1.71	0.13	0.70	0.05	41.17	c
BMW104925.3+324639	10 49 25.13	+32 46 27.1	p	PGC 0039328	NGC 4224	Sa	53	12.35	5.79	1.06	2.37	0.43	40.88	C1
BMW110522.3+381421	11 05 23.18	+38 14 13.2	p											
BMW113446.5+485718	11 34 46.51	+48 57 17.6	p											
BMW113448.9+490440	11 34 49.51	+49 04 39.6	p											
BMW114223.6+101552	11 42 23.79	+10 15 51.2	p											
BMW114232.1+583706	11 42 32.04	+58 37 05.8	p											
BMW114430.3+305305	11 44 30.20	+30 53 02.9	p											
BMW115535.8+232724	11 55 35.92	+23 27 27.5	p											
BMW120438.2+014717	12 04 38.50	+01 47 10.5	p											
BMW120631.5-295119	12 06 31.46	-29 51 18.7	p											
BMW121049.5+392822	12 10 49.82	+39 28 23.9	p											
BMW121049.5+392820														
BMW121049.6+392823														
BMW121633.3+072746	12 16 34.07	+07 27 46.9	p											

BMW121908.2+470531	12 19 08.40	+47 05 20.5	p	PGC 0039615	UGC 7356	Irr	8	15.35	1.87	0.47	0.96	0.17	38.65	
BMW122018.0+752214	12 20 17.39	+75 22 16.6	e	40	PGC 0039791	NGC 4291	E	44	12.04	13.65	1.37	6.01	0.60 41.11	
BMW122503.5+125317	12 25 04.23	+12 53 07.5	e	100	PGC 0040455	NGC 4374	E	25	9.84	54.48	2.77	23.97	1.22 41.23 Cl	
BMW122504.1+125308														
BMW122504.3+125318														
BMW122504.4+125316														
BMW122504.4+125319														
BMW122611.1+125642	12 26 11.68	+12 56 45.2	e	200	200 400	PGC 0040653	NGC 4406	E	25	9.73	199.80	7.89	87.91	3.47 41.79 Cl
BMW122612.6+125628														
BMW122716.2+085815	12 27 14.97	+08 58 17.3	e	80	PGC 0094216			530	16.11	3.74	1.03	1.53	0.42 42.73 Cl	
BMW123017.6+121936	12 30 17.59	+12 19 35.7	e	30	PGC 0041297	NGC 4478	E	25	11.93	1.31	0.30	0.68	0.13 39.63 Cl	
BMW123018.1+121926														
BMW123052.5+143307	12 30 52.51	+14 33 06.7	e	40	PGC 0169455	VPC 774			18.18	7.98	1.43	3.51	0.63	
BMW123643.2+131515	12 36 43.14	+13 15 19.0	p	PGC 0042081	IC 3583	Irr	25	13.11	0.67	0.32	0.30	0.14	39.33 Cl	
BMW124342.7+162340	12 43 42.68	+16 23 38.0	p	PGC 0042833	NGC 4651	Sc	25	10.81	1.30	0.36	0.53	0.15	39.55 c; Cl	
BMW125232.8-153057	12 52 33.03	-15 31 02.2	p	PGC 0043675	MCG -2-33-38	S0	87	14.39	3.19	0.31	1.50	0.14	41.11 c; Gr	
BMW125233.1-153102														
BMW125302.3-152120	12 53 02.26	-15 21 19.7	p	PGC 0043748	DRCG25-68	E-S0	266	15.55	0.54	0.20	0.25	0.09	41.38 Cl	
BMW125318.1-153203	12 53 18.27	-15 32 03.4	e	30	PGC 0043777	DRCG25-39	E-S0	284	14.78	2.94	0.34	1.38	0.16 42.11 Cl	
BMW125318.3-153203														
BMW125749.0-171628	12 57 49.85	-17 16 25.3	e	50	PGC 0044369		E	296	14.77	13.80	1.77	6.76	0.87 42.84 Cl	
BMW125750.2-171616														
BMW130055.7+274740	13 00 55.99	+27 47 29.8	p	PGC 0044840	NGC 4911	SBbc	159	13.30	12.83	1.03	4.74	0.38	42.14 Cl	
BMW130056.0+274737														
BMW130056.2+274731														
BMW130559.7+291647	13 05 59.46	+29 16 46.8	p	PGC 0045318	CGCG 160-136	E	159	15.08	4.42	0.95	1.64	0.35	41.66 c	
BMW130803.0+292918	13 08 03.09	+29 29 12.0	p	PGC 0166974					2.61	0.17	0.97	0.06	Cl?	
BMW130803.2+292910														
BMW130803.3+292911														
BMW130803.4+292903														
BMW131324.5-325247	13 13 24.96	-32 52 44.7	p	PGC 0158561					16.26	1.12	0.41	0.55	0.20	
BMW131413.5-425739	13 14 13.44	-42 57 38.8	e	60	PGC 0046023	NGC 5026	SBa	75	11.73	86.49	3.71	47.57	2.04 42.48 Cl?	
BMW131912.4-123228	13 19 12.40	-12 32 28.1	e	20	PGC 0046432	NGC 5072	E-S0	136	14.23	2.09	0.74	0.92	0.33 41.27 c	
BMW132040.2-434200	13 20 40.20	-43 42 00.3	p	PGC 0046566	NGC 5082	S0	78	12.96	0.93	0.50	0.51	0.27	40.54 Gr	
BMW132745.6-314751	13 27 45.41	-31 47 54.0	p	PGC 0047177					265	14.53	3.74	0.61	1.76	0.29 42.15 Cl
BMW132759.6-272104	13 27 59.87	-27 21 29.6	p	PGC 0047209	IC 4255	E	203	13.66	3.91	1.11	1.92	0.55	41.95 Cl	
BMW132802.6-314519	13 28 02.56	-31 45 19.0	p	PGC 0088857		E	258	15.01	3.37	0.60	1.58	0.28	42.08 Cl	
BMW132958.2+471613	13 30 00.20	+47 15 55.1	e	80	PGC 0047413	NGC 5195	SBpec	14	10.10	12.66	0.77	5.19	0.32 40.06 Gr	
BMW132959.1+471555														
BMW132959.8+471556														
BMW133000.1+471558														
BMW133006.4-014316	13 30 06.34	-01 43 06.8	e	45	PGC 0047432	NGC 5183	Sb	86	13.21	2.86	0.98	1.17	0.40 41.04 c	
BMW133425.1+344127	13 34 24.86	+34 41 26.9	e	60	PGC 0047822	NGC 5223	E	144	13.22	20.33	1.70	7.52	0.63 42.24 Cl	
BMW134623.6-375810	13 46 23.36	-37 58 23.3	p	PGC 0048817	ESO 325-G16				228	14.67	11.43	1.27	5.37	0.60 42.48 Cl
BMW135321.7+402151	13 53 21.67	+40 21 50.7	p	PGC 0049347	NGC 5350	SBbc	57	11.87	1.38	0.40	0.51	0.15	40.26 Gr	
BMW140715.2-270922	14 07 15.27	-27 09 27.7	e	30	PGC 0050373	ESO 510-G66	E-S0	146	13.97	9.04	0.77	4.43	0.38 42.03 Cl	
BMW141319.7-030857	14 13 19.76	-03 08 58.0	p	PGC 0050786	NGC 5507	SO	43	13.22	0.31	0.09	0.14	0.04	39.47	
BMW144104.0+532011	14 41 04.03	+53 20 10.7	p	PGC 0084264					629	17.53	5.88	1.02	2.18	0.38 42.99
BMW151643.2+552432	15 16 42.26	+55 24 22.2	p	PGC 0054522	NGC 5908	Sb	66	12.20	0.53	0.20	0.20	0.07	39.92	
BMW160434.7+174315	16 04 34.65	+17 43 21.9	e	300	PGC 0056962	NGC 6041	E-S0	209	13.90	183.30	4.47	80.65	1.97 43.60 Cl	

BMW160435.9+174325
 BMW160508.1+174528 16 05 07.32 +17 45 27.4 p
 BMW160508.2+174340 16 05 08.28 +17 43 44.9 p
 BMW160508.5+174344
 BMW160533.6+173611 16 05 32.96 +17 35 58.8 e 40
 BMW160534.4+323942 16 05 34.64 +32 39 37.4 p
 BMW160544.5+174303 16 05 44.49 +17 43 02.4 p
 BMW161533.6-603948 16 15 32.22 -60 39 55.3 p
 BMW161546.1-605509 16 15 46.04 -60 55 08.7 p
 BMW161720.2+345408 16 17 20.23 +34 54 07.9 e 20
 BMW165944.0+323656 16 59 44.21 +32 36 58.2 e 50
 BMW171305.9+434202 17 13 05.49 +43 42 02.2 p
 BMW171519.1+573932 17 15 18.99 +57 39 33.5 p
 BMW173356.4+433936 17 33 56.58 +43 39 30.9 p
 BMW174336.7+330457 17 43 37.14 +33 04 57.9 p
 BMW181055.5+500049 18 10 54.76 +50 00 48.0 p
 BMW184359.5+453851 18 43 59.70 +45 38 55.0 e 30
 BMW190012.7-362702 19 00 12.47 -36 27 04.6 p
 BMW192131.5+435941 19 21 31.81 +43 59 41.4 p
 BMW201127.3-564408 20 11 27.57 -56 44 05.5 p
 BMW201214.3-563822 20 12 14.71 -56 38 16.4 p
 BMW204843.3+251650 20 48 43.29 +25 16 49.8 p
 BMW210716.0-252807 21 07 16.01 -25 28 7.2 p
 BMW210720.4-252917 21 07 20.05 -25 29 16.2 p
 BMW215209.2-194323 21 52 09.58 -19 43 22.7 e 20
 BMW215209.4-194318
 BMW221818.1-593625 22 18 18.55 -59 36 23.4 p
 BMW223633.3+343010 22 36 32.97 +34 30 09.2 p
 BMW223718.9+342654 22 37 19.17 +34 26 55.7 p
 BMW231221.4-435145 23 12 21.96 -43 51 53.2 p
 BMW231546.1-590313 23 15 45.97 -59 03 11.3 p
 BMW231713.2+184229 23 17 11.37 +18 42 32.8 e 80
 BMW231756.7-421339 23 17 56.23 -42 13 32.5 p
 BMW231855.6-421406 23 18 55.60 -42 14 05.9 e 30
 BMW231855.6-421359
 BMW231921.5-415910 23 19 21.75 -41 59 02.9 p
 BMW231921.5-415906
 BMW232042.7+081305 23 20 42.72 +08 13 05.1 p
 BMW233842.8+271300 23 38 42.74 +27 12 59.7 p
 BMW234818.3+010623 23 48 18.80 +01 06 24.0 p
 BMW234823.7-280427 23 48 23.98 -28 04 24.3 p
 BMW234847.1-281217 23 48 46.73 -28 12 18.8 p
 BMW235415.0-100955 23 54 14.53 -10 09 52.0 e 55
 BMW235415.1-100950

PGC 0057031	NGC 6045	SBc	204	13.58	1.12	0.25	0.49	0.11	41.37	C1
PGC 0057033	NGC 6047	E	188	14.10	6.43	0.52	2.83	0.23	42.05	C1
PGC 0057062	IC 1178	E-S0	204	14.74	2.57	0.53	1.13	0.24	41.71	C1
PGC 0057078	CGCG 195-013	Sc		15.29	2.12	0.44	0.87	0.18	c	
PGC 0057096	IC 1185	Sab	208	14.47	5.61	0.51	2.47	0.23	42.09	C1
PGC 0057637	ESO 137-G7	E-S0	100	13.08	8.95	1.48	8.33	1.38	41.96	C1
PGC 0057649	ESO 137-G8	E	77	12.28	6.43	0.71	5.98	0.66	41.60	C1
PGC 0057728	NGC 6107	E	184	14.26	4.32	0.45	1.77	0.18	41.84	c; Gr
PGC 0059392			591	15.71	30.20	3.62	12.38	1.48	43.71	C1
PGC 0059859	CGCG 225-70		330	15.75	4.68	0.55	1.92	0.22	42.37	
PGC 0059942	MCG 10-24-118		168	16.13	4.99	0.72	2.20	0.32	41.85	
PGC 0060505	CGCG 226-29			16.31	1.84	0.49	0.81	0.21		
PGC 0060757	CGCG 199-10			15.73	4.30	0.85	2.02	0.40		
PGC 0061505	MCG 08-33-27	E-S0	296	14.85	1.24	0.41	0.58	0.19	41.77	C1?
PGC 0165780			263	16.00	1.22	0.42	0.62	0.21	41.67	
PGC 0209730	CGMW 4-4359			4.03	0.98	2.22	0.54			
PGC 0063122	CGCG 230-9	Sc	273	13.81	10.83	1.75	5.96	0.96	42.70	c; C1
PGC 0064228		E	324	15.74	8.58	0.59	4.20	0.29	42.70	C1
PGC 0095814				17.37	5.05	0.50	2.48	0.25	C1?	
PGC 0065435	MCG 04-49-3	E-S0	291	17.00	3.62	0.46	2.10	0.27	42.30	C1
PGC 0066136	NGC 7016	E	219	14.28	10.18	1.04	4.99	0.51	42.42	C1
PGC 0066137	NGC 7017	SO	222	14.24	4.18	0.83	2.05	0.41	42.07	C1
PGC 0067523	ESO 600-G14	SO-a	581	15.36	2.12	0.45	0.93	0.20	42.54	C?
PGC 0068536	IC 5187	Sc		14.86	5.57	1.08	2.28	0.44	c	
PGC 0069291			174	(16.60)	1.30	0.36	0.72	0.20	41.38	
PGC 0069338	NGC 7335	SO-a	126	13.90	1.10	0.32	0.60	0.18	41.03	c; Gr
PGC 0070684	ESO 291-G6	E-S0		15.14	2.27	0.73	0.93	0.30	C1?	
PGC 0070861	ESO 148-IG2	Sm	268	14.76	1.80	0.49	0.79	0.21	41.81	c
PGC 0070934	NGC 7578B	E	241	14.21	43.44	2.43	21.28	1.19	43.14	Gr
PGC 0131791		SO-a	336	15.63	0.53	0.27	0.22	0.11	41.41	Gr?
PGC 0071031	NGC 7590	Sbc	26	11.37	3.44	0.58	1.41	0.24	40.03	Gr
PGC 0095173		Sa		16.00	2.12	0.65	0.87	0.27	Gr?	
PGC 0071140	NGC 7626	E	69	11.92	5.55	1.05	2.72	0.51	41.16	C1
PGC 0071994	CGCG 476-95	E	186	14.76	0.52	0.25	0.25	0.12	40.89	C1
PGC 0196693			584	16.46	0.34	0.20	0.16	0.09	41.89	
PGC 0072471	DUKST 471-12	SO	203	14.64	3.61	0.87	1.48	0.36	41.84	C1
PGC 0085790	DRCG54-31	SO		16.14	5.17	1.22	2.12	0.50	C1?	
PGC 0141285		Sbc	394	16.29	3.75	0.62	1.65	0.27	42.47	C1